ACS APPLIED MATERIALS & INTERFACES

Research Article

www.acsami.org

Reinforced Carbon Nanotubes as Electrically Conducting and Flexible Films for Space Applications

Nurit Atar,*[,†,‡] Eitan Grossman,[†] Irina Gouzman,[†] Asaf Bolker,[†] and Yael Hanein[‡,§]

[†]Space Environment Department, Soreq NRC, Yavne 81800, Israel

[‡]School of Electrical Engineering, Tel-Aviv University, Ramat Aviv, Tel-Aviv 69978, Israel

[§]Tel-Aviv University Center for Nanoscience and Nanotechnology, Tel-Aviv University, Ramat Aviv, Tel-Aviv 69978, Israel

ABSTRACT: Chemical vapor deposition (CVD)-grown entangled carbon nanotube (CNT) sheets are characterized by high electrical conductivity and durability to bending and folding. However, since freestanding CNT sheets are mechanically weak, they cannot be used as stand-alone flexible films. In this work, polyimide (PI) infiltration into entangled cup-stacked CNT (CSCNT) sheets was studied to form electrically conducting, robust, and flexible films for space applications. The infiltration process preserved CNTs' advantageous properties (i.e., conductivity and flexibility), prevented CNT agglomeration, and enabled CNT patterning. In particular, the CNT-PI films exhibited ohmic electrical conductance in both the lateral and vertical directions, with a sheet resistivity as low as 122 Ω/□, similar to that of as-grown CNT sheets, with minimal effect of the insulating matrix. Moreover, this high conductivity was preserved under mechanical and thermal manipulations. These properties make the reported CNT-PI films excellent candidates for applications where flexibility, thermal stability, and electrical conductivity are required. Particularly, the developed CNT-PI films were found to be durable in space environment hazards such as high vacuum, thermal cycling, and ionizing radiation, and hence they are suggested as an alternative for the electrostatic discharge (ESD) protection layer in spacecraft thermal blankets.

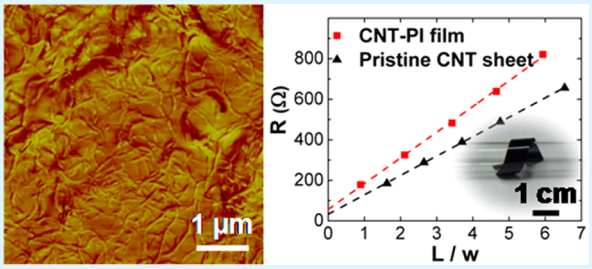

KEYWORDS: *CNT sheets, polyimide, nanocomposites, electrical conductivity, space environment*

1. INTRODUCTION

Electrically conductive, flexible, and lightweight materials are needed in various applications, including interconnects in electronics, field emission devices, electrostatic discharge (ESD) prevention, and electromagnetic interference (EMI) shielding. Protection from ESD is particularly important in space environment due to charging of the external insulating surfaces of the spacecraft as a result of space plasma exposure. This challenge is especially critical in the geo-synchronous earth orbit (GEO) used for communication satellites.[1] Electrostatic charge (ESC) accumulation may damage the spacecraft electronics through sudden electrical discharge.

A common solution is imparting surface conductivity to insulating polymer films by depositing electrically conductive coatings, where the antistatic criterion to dissipate ESC build-up requires surface resistivity in the range of 10^6–10^{10} Ω/□. Indium tin oxide (ITO) is usually applied as an electrically conducting coating for space applications, e.g., ITO-coated polyimide (PI) is used as an exterior layer for spacecraft thermal control blankets. PI is used in various applications, ranging from microelectronics to space applications owing to its excellent radiation and chemical resistance as well as its thermal stability.[2] It is a highly durable polymer under space hazards, i.e., UV radiation, ionizing radiation, ultrahigh vacuum, and harsh temperature cycles.[1] While the deposition of ITO on PI improves the film conductivity, it severely diminishes its flexibility owing to the brittle nature of ITO, which cannot tolerate folding or bending into small diameters. Mechanical robustness tests applied to ITO-coated films have resulted in immediate loss of sheet conductivity due to fracture of the coating upon bending.[3]

A different approach to form flexible, electrically conducting films is based on polymers incorporating electrically conductive additives at a concentration above the percolation threshold. Due to their extraordinary electrical properties, carbon nanotubes (CNTs) have been widely explored as additives for electrical conductivity enhancement of polymers.[4] CNTs are advantageous compared to other conductive additives owing to their extremely high aspect ratio and high conductivity, enabling lower CNT loadings. CNT-based composites have indeed shown promise in applications such as touch/pressure sensors, field emitters, ESD and EMI shielding, and photovoltaic devices.

CNTs of various nanostructures such as bamboo, herring-bone and cup-stacked can be used. Specifically, cup-stacked CNTs (CSCNTs),[5] which were investigated in this work, exhibit a unique morphology of stacked, truncated graphene

Received: September 2, 2014
Accepted: November 3, 2014
Published: November 3, 2014

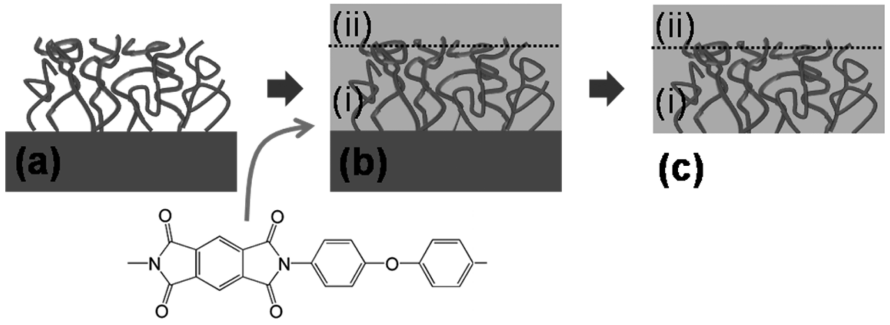

Figure 1. Schematic illustration of CNT-PI film fabrication process: (a) ~9 μm thick CNT sheet is first grown by CVD on a prepatterned Si substrate. (b) PI (PMDA-ODA monomer) is then infiltrated into the CNT sheet. (i) Type 1 samples were cast by ~9 μm thick PI layer (up to the dotted line). (ii) Type 2 samples were prepared with excess of PI layer (~15 μm thick). (c) Finally, free-standing CNT-PI film is mechanically peeled off the substrate.

cones along the tube axis. Evidence for linear[6] and nonlinear[7] current versus voltage curves was found.

Since CNTs are not easily soluble in polymeric solutions, they tend to agglomerate as bundles within the polymer matrix. Accordingly, common incorporation methods are based on dispersion of CNT powder in polymer matrices using sonication and functionalization to improve homogeneity.[4] The electrical conductivity of composites made from CNT dispersion is affected by the incorporation procedures (e.g., sonication) that often result in severe degradation of the original CNT properties (e.g., electrical, thermal, and mechanical characteristics).[4] Additionally, the electrical conductivity of dispersed systems is inferior since the CNT network is formed in the presence of an insulating polymer, which tends to hamper the intertube electrical contacts. Improving the composite electrical conductivity by enlarging the CNT content is problematic as forming homogeneous dispersions and removing large amounts of solvents are challenging, often resulting in degradation of mechanical properties. Indeed, CNT-PI composites from dispersions[8−13] are generally characterized by limited conductivity (up to 0.1 S/cm at a CNT loading of 3.7 vol % and film thickness of about 40 μm).[9] High conductivities can be reached for composites prepared by dispersion process; for example, Yuan et al.[14] reported conductivity of 38.8 S/cm for a 15 μm thick CNT-PI film with a nanotube loading of 30 wt %.

Many recent studies sought simple methods to control CNT distribution within a polymer matrix, while protecting the CNT properties. An alternative fabrication technique uses polymer solution infiltration into chemical vapor deposition (CVD)-grown aligned CNT sheets.[15−17] The aligned CNT-polymer composites allow primarily top-to-bottom conductive routes owing to their anisotropic structure. Since the CNTs are fixed on a substrate, no CNT agglomeration takes place. Hence, destructive treatments for homogeneous distribution, commonly applied in CNT powder dispersions, are avoided when CNT sheets are used. The state of the art conductivity for CNT-PI films, 183 S/cm, was achieved by PI infiltration into aligned, pulled-out CNT sheets.[18] However, the unidirectional CNT structure leads to an anisotropic (longitudinal) conductivity nature, as well as low ductility.

In this study, we describe the use of entangled CVD grown CSCNT sheets as a building block to form flexible, free-standing CNT-PI films with high isotropic electrical conductivity as a flexible alternative for ESD protection layers in the space environment. Entangled CNT sheets composed of numerous random CNT junctions were infiltrated by PI solution, which was used to provide mechanical stability, robustness, and flexibility to the original porous CNT structure, resulting in flexible and electrically conductive CNT-PI films.

Compared with CNT-PI composites with higher electrical conductivity,[14,18] the films reported here demonstrate 0.2 S/cm isotropic conductivity at 14 vol %. However, the present preparation method enables preservation of the original CNT sheet conductivity with no degradation related to the insulating PI matrix. Hence, higher electrical conductivity can be easily reached, for example, by controlling the CVD process to form denser CNT sheets with higher conductivities. Another advantage of the technique presented here is the compatibility with patterning of CNT along the composites, which is not facilitated by the dispersion technique.

The films were found durable to GEO conditions by exposure to simulated space environment (vacuum, thermal cycles, and ionizing irradiation). The dimensions of the films are scalable and can be customized by a common sewing technique for spacecraft thermal blankets. Therefore, the CNT-PI films reported here represent a novel and viable alternative for ESD protection layer in spacecraft thermal blankets.

2. EXPERIMENTAL METHODS

2.1. Materials. Polyamic acid (PAA) solution of pyromellitic dianhydride-oxidianiline (PMDA-ODA) 15 wt % in *N*-methyl-2-pyrrolidone (NMP) (Sigma-Aldrich, 575801) formed the PI matrix. CSCNT sheets were grown by the CVD technique on Si wafer with 500 nm thermal oxide layer (SiO_2). Substrates were coated with 25 Å thick Ni as a catalyst layer by electron beam evaporation. The CVD process included gradual increase of furnace temperature to 900 °C within 20 min and growth duration of 5 min under hydrogen and ethylene flow of 1000 and 20 sccm, respectively. The volume fraction of the grown CNTs within the porous sheet was calculated from its mass and the total sheet volume, assuming specific gravity of 1.8 g/cm^3.[4] The mass of pristine CNT sheets was measured by microbalance, Sartorius SE2 (readability of ±0.1 μg), and its thickness was determined by scanning electron microscopy (SEM). The resulting thickness of the CNT sheets was 9 ± 2 μm and the CNT content in the sheets was calculated to be 14 vol %. Patterned CNT sheets were realized with Ni islands that were prepatterned using photolithography.[19]

2.2. Nanocomposite Films Preparation. PI was designated as a solid matrix to impart mechanical robustness and flexibility to the porous CNT structure. PAA solution was infiltrated into the CSCNT sheets as shown schematically in Figure 1a (including the chemical structure of PMDA-ODA PI monomer). Following the PAA cast, a full penetration of the PAA between the CNTs was achieved (Figure 1b) and the PAA-CNT systems were heated. The PAA solution was cured into PI by gradual heating to 350 °C in nitrogen atmosphere, based on

a process developed by DuPont, Inc.[20,21] During heating, the NMP was evaporated; thus, the resulting PI thickness is one tenth of the initial PAA thickness.

Since the PI infiltration was governed by the polymer viscosity and CNT wettability, two different infiltration methods were used according to the sample size. Type 1 samples were characterized by small area of up to 4 cm^2 and PI film thickness was about 9 μm after curing. PAA solution (0.15 mL) was first poured over the surface of the CNT sheet and then spin coated at 3500 rpm (SPIN 150, SPS). Larger samples of up to 14 cm^2, further denoted as CNT-PI films of type 2, were fabricated using a PAA diluted in NMP (PAA:NMP ratio of 1:3) to improve control over the thickness and the homogeneity of the resulting films. Diluted PAA was poured on large CNT sheets (67 $\mu L/cm^2$). The total CNT-PI film thickness after curing was 15 ± 2 μm with only the bottom 9 ± 2 μm layer containing CNTs. The thicker PI layer in type 2 samples was designed for improved mechanical robustness. Samples larger than 14 cm^2 can be prepared depending on the CVD reactor size thanks to the stability of the supporting polymer. Type 1 samples were used to characterize the films' top-to-bottom electrical properties (bulk conductivity and current-versus-voltage measurements), while type 2 samples were used for measuring sheet resistivity and current-versus-voltage along the lateral direction.

Free-standing flexible CNT-PI films were obtained by peeling the nanocomposites from the substrate (Figure 1c). Easy peeling was enabled due to decreased adhesion between the CNTs and the oxide layer on the Si wafer.

2.3. Morphological Observation. The CNT structure was examined by transmission electron microscopy (TEM; Jeol JEM 2100, 200 keV) to determine the CNT type, diameter, and wall number. The morphology of the pristine CNT sheets was characterized by high resolution scanning electron microscopy (HRSEM; Magellan, FEI Co.) and that of the CNT-PI films by environmental scanning electron microscopy (ESEM; Model Quanta 200, FEI Co.) and atomic force microscopy (AFM; MultiMode, Nanoscope IV, Veeco Instruments Inc.). Wetting of the CNT sheets by the PI solution was validated by analyzing the elemental composition of the nanocomposite's surface by energy dispersive spectroscopy (EDS; EDAX) to assess the PI solution penetration.

2.4. Mechanical Characterization. Tensile tests were performed using DMA Q800 from TA Instruments and the data was analyzed by the included Universal Analysis 2000 software version 4.5A. Typical stress versus strain curves were obtained at room temperature. The procedure includes control over the applied force with a rate of 3.00 N/min. The measured samples were cut to 11.10×5.01 mm^2 (type 2). The maximal stress that the films withstand before failing was reported as the tensile stress. Young's Modulus was calculated as the slope of the stress versus strain curve in the linear range.

2.5. Electrical Property Characterization. *2.5.1. Microscopic Electrical Analysis.* The microscopic electrical properties of the CNT-PI films were evaluated using conductive AFM (C-AFM). The C-AFM module operates in contact mode and performs both morphology and current imaging in a single scan. Using C-AFM, the top-to-bottom current through the CNT-PI films was measured at room temperature. Scanning was conducted while applying DC bias between a conductive tip (antimony doped Si with Co/Cr coating, MESP model from Bruker) and a 5×5 mm^2 CNT-PI film. The resulting C-AFM images were analyzed by scanning probe microscopy software (WSxM, Nanotec Electronica[22]). C-AFM was also used to obtain current versus voltage curves by measuring the top-to-bottom current through the sample as a function of the applied DC bias.

2.5.2. Macroscopic Electrical Analysis. The macroscopic electrical properties of the samples in the lateral direction were measured using a source meter (Kiethley 2400, Keithley Instruments). The source meter probes were attached to parallel silver paint (5001-AB, SPI Supplies) electrodes that were applied on the surface of the samples. In another nondestructive configuration, aluminum bar electrodes were pressed on the sample surface using a weight instead of irreversibly marking the sample. The DC current was supplied and the built-up voltage was measured for both current versus voltage and resistivity measurements in the lateral direction. To perform sheet resistivity measurements, a set of parallel electrodes was applied across the surface of a 0.5×4 cm^2 sample to form several square segments with area of about 25 mm^2 each. The sheet resistance, R, was measured for different areas with a constant width (5 mm), w, and increasing length, L (up to 4 cm). The sheet resistivity, ρ_s, in units of $\Omega/\square$ (ohm per a single square segment) is related to the sheet resistance according to the relation:

$$R = \rho_s \frac{L}{w} \tag{1}$$

A trend line that was fitted to the resistance versus the number of measured segments, L/w. ρ_s, was calculated as the linear-line's slope, and the contact resistance was expressed by its intercept with the y-axis.

The sheet resistivity measurement described above was repeated after winding cycles to examine the durability of the electrical conductivity of the CNT-PI films under mechanical manipulations. The films were wound manually up to 300 times around a ceramic rod of 2.9 mm diameter and their resistivity was measured after each winding cycle.

In addition, the temperature dependence of the sheet resistivity was measured by van der Pauw four-point probe method that eliminates influence of the contact resistance and sample geometry on the measurement.[23] The sample temperature in the range of −160 to 200 °C was controlled using a THMS600 Linkam stage working in nitrogen atmosphere. The current was supplied using a Keithley 220 programmable current source and measured using a Keithley 485 picoammeter. Four silver contacts were applied by spreading silver paint dots on the corners of 5×5 mm^2 samples. Each of the four contacts was connected to a very high input impedance (TΩ) electrometer (Keithley 6514). The voltage difference between each of the two electrometers was measured using a Keithley 2000 multimeter. The current source, electrometers, multimeter, and sample contacts were connected to a Keithley 7001 switch. All elements in the system were controlled using a computer.

2.6. Durability to GEO Space Environment. *2.6.1. Outgassing under Heating and Vacuum.* A standard test method, ASTM E595-07,[24] was used to approve the CNT-PI films as low-outgassing materials for vacuum environment. Samples were held for 24 h at a temperature of 125 °C and pressure of less than 1×10^{-5} Torr. Comparing the initial and final mass of the samples yields the total mass loss (TML). During the outgassing test, a collecting plate was held at 25 °C to measure the amount of collected volatile condensable material (CVCM). The low-outgassing criterion requires TML of less than 1% and CVCM lower than 0.1%. Mass gain/loss was measured by microbalance, Sartorius SE2 (readability of 0.1 μg).

2.6.2. Thermal Cycling. The durability of the electrical conductivity of the CNT-PI films (type 2, 5×5 mm^2) was tested by four-point van der Pauw technique under thermal cycles in the range of −100 to 140 °C, corresponding to extreme thermal conditions—shade and direct solar illumination. The thermo-optical characteristics of the CNT-PI films, solar absorptance, α_s, and thermal emittance, ε, were measured by IR/solar reflectometer (TESA 2000, AZ technology) using an integrating sphere.

2.6.3. Ionizing Radiation. The GEO environment is commonly simulated by exposure to γ radiation,[25,26] which is also a form of ionizing radiation[1] since, according to Compton effect, the γ rays are scattered by electrons, producing secondary electrons. Exposure to low γ radiation doses, up to tenths of kGy, was performed in a Pb−Al cylinder using a ^{60}Co source (gamma cell 220 type B from Nordion International Inc., with spectral peaks at 1.33 Mev and 1.17 Mev) in atmosphere at room temperature. The precise dose rate, 41.44 Gy/h, was determined by ionization chamber dosimeter from PTB. An additional ^{60}Co source was used to obtain high irradiation doses, with dose rate of 0.1 MGy/h for a sample distance of 7 cm, as measured by a perspex dosimeter (Harwell Dosimeters Ltd.). CNT-PI films (type 2, 0.5×4 cm^2) were gradually exposed to a total radiation dose of 9.9 MGy, equivalent to about 15 years in GEO, which is characterized by a total irradiation dose of 0.7 MGy/year.[27] The γ radiation influence on the electrical resistivity of the films was measured after each dose increment.

3. RESULTS AND DISCUSSION

3.1. Structure Characterization. CNT sheets were grown by CVD on Si substrates in 9 ± 2 μm thick entangled networks. A top view HRSEM image (Figure 2a) of an as-grown CNT sheet demonstrates an entangled isotropic nature. Individual CNTs were studied by TEM (Figure 2b) and found to have CSCNT structure, in which truncated open-ended graphene cones are stacked to form a tubular nanostructure. The outer diameter of ~20 individual CNTs was measured as 22 ± 2.02 nm and the distance between neighboring graphene layers was ~3.5 Å, in good agreement with CSCNT structure.[5] The typical TEM image shows that the multiple graphene layers that assemble the CNT structure are positioned relative to the tube axis with an angle, θ, that varies between 15 and 25 degrees. In addition, open edges of graphene layers were observed on both the inner and outer surface of the hollow tube (marked with black arrows), as expected from a CSCNT structure.[28] The existence of the incline angle may be explained by the relatively high content of hydrogen in the growth process. Hydrogen was assumed to enable the cup-stacked structure with open edges of graphene layers since it satisfies the valences at the cone edges.[29] This characteristic makes CSCNTs advantageous as additives since the numerous dangling bonds along the CNT give rise to a high chemical reactivity and improved bonding to polymers.[30] The superior wettability of the CSCNTs has a significant influence on the flexibility of the composite film because of improved bonding between the CNTs and the flexible supported matrix. The existence of the dangling bonds and the lack of covalent bonding between adjacent cones results in inferior electrical conductivity of individual CSCNT, around 5 × 10^{-3} Ωcm[6] (1 order of magnitude lower than MWCNT[30]). However, for an ESD protection application this electrical conductivity is adequate.

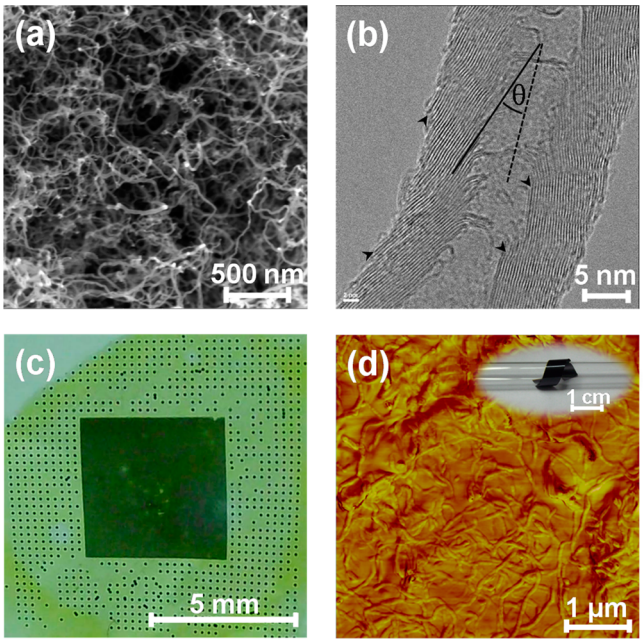

Figure 2. (a) Top view HRSEM image of an as-grown entangled CNT sheet. (b) TEM image of a typical cup-stacked CNT. (c) Optical microscope image of a patterned, free-standing CNT-PI film (type 2) with area of 1 × 1.5 cm^2 and 10 μm thickness. (d) AFM phase image of the top surface of a CNT-PI film (type 1). Inset: Optical microscope image of a free-standing CNT-PI nanocomposite film (type 2, 17 μm thick, 0.5 × 3.5 cm^2 area) wrapped around a glass tube (7 mm diameter).

PI was infiltrated into the CNT sheets to fill the pores and to function as a mechanically supporting matrix of a CNT-PI flexible film. Such CNT-PI freestanding films were prepared by PI infiltration into CNT sheets, cured, and peeled from the Si substrates. In addition to the formation of uniform CNT-PI films, patterned CNT-PI films were produced from patterned CNT sheets that were grown by CVD on prepatterned islands of Ni catalyst. Patterned CNT-PI free-standing films with two different patterns were realized, as shown in Figure 2c, by infiltration method type 2 (described in the Experimental Methods). The exterior pattern includes CNT islands (120 μm diameter). The interior region (shown as a black square) is a dense hexagonal pattern of CNT islands (20 μm diameter).

The flexibility of the CNT-PI films is demonstrated in the inset of Figure 2d, which depicts a free-standing CNT-PI film wrapped around a 7 mm diameter glass tube. The penetration of the PI through the CNT sheets was validated by PI presence at the bottom surface (indicated by a nitrogen signal in the elemental analysis, EDS; data not shown). The top surface morphology of the type 1 CNT-PI films was examined by AFM (Figure 2d). A homogeneous distribution of CNTs in a PI matrix is clearly visualized. This result indicates that the preparation procedure preserves the homogeneous structure of the entangled CNT sheet without agglomerates in spite of the PI infiltration. The revealed CNT junctions on the film surface are part of the CNT network that enables electrical conductivity along the film surface. In addition, the flexibility of the CNT-PI film is related to the complete PI coverage, which is observed in the AFM image with no indication of air voids.

The CNT-PI films demonstrated Young's modulus of 2.3 GPa, close to that of the pristine PI matrix (2.5 GPa).[31] The tensile strength of the CNT-PI films was found to be 80 MPa, lower than that of the pristine PI (231 MPa).[31] However, this tensile strength is adequate for ESD protection since thermal blankets are exposed to minor tensile stresses. The durability to bending, the relevant mechanical property for thermal blanket application, was examined as presented below.

3.2. Electrical Characterization. The microscopic electrical properties of the freestanding CNT-PI films were characterized by C-AFM, where the top-to-bottom electrical current through the sample is mapped at nanometer resolution. An electrical current flow through the films was measured for type 1 samples (the thickness of the PI is slightly less than the CNT sheet thickness). A typical C-AFM image, shown in the inset of Figure 3a, demonstrates many top-to-bottom routes with electrical conduction (bright spots) under 100 mV bias. Differences in the measured electrical current, visualized from the brightness of the distinctive spots, may be related to variation in the total length of the conducting route as well as the number of CNT junctions or thickness of PI coverage. Analysis of the C-AFM image revealed 509 conducting elements with 153 nm first-neighbor distance and a total conducting area of 3.52 μm^2, amounting to 14.2% of the scanned area (5 × 5 μm). A typical C-AFM current versus voltage curve for a single top-to-bottom route (Figure 3a) shows ohmic resistance, indicating a metallic electrical conductance through top-to-bottom CNT routes.

Current versus voltage in the lateral direction and sheet resistivity were examined for type 2 CNT-PI films. These CNT-

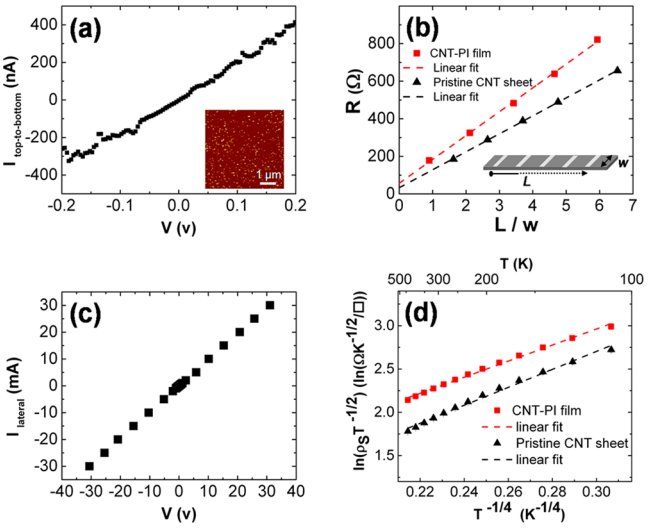

Figure 3. Electrical properties of CNT-PI films and pristine CNT sheets. (a) Current versus voltage curve measured from top-to-bottom by C-AFM for a single conducting route of a 10 μm thick CNT-PI film. Inset: C-AFM top-to-bottom current image (full scale: 300 nA) of the CNT-PI film. Bright spots indicate top-to-bottom conducting routes. (b) Sheet resistance of a CNT-PI film (red squares) and pristine CNT sheet (black triangles) as a function of the number of measured squares (L/w) with sheet resistivities of 127 and 96 Ω/□, respectively, calculated as the slope of the corresponding linear fit. The total area of both samples was 0.5 × 4 cm^2. (c) Current versus voltage curve along the lateral direction of a CNT-PI film (0.5 × 4 cm^2 area). (d) Temperature-dependent sheet resistivity of 5 × 5 mm^2 CNT-PI film (red squares) and pristine CNT sheet (black triangles).

PI films were 17 μm thick and consisted of a 9 μm CNT layer (embedded in PI) and an additional 8 μm thick PI layer on top.

The macrospcopic sheet resistance of the CNT-PI films and CNT sheets, R, was measured for different areas with a constant width (w = 5 mm) and increasing length (L = 0.5 to 4 cm). The sheet resistivity, ρ_s was calculated according to (1) as the slope of the linear trend line of the experimental data (R versus L/w). Typical measured data are plotted in Figure 3b with red squares and black triangles for a CNT-PI film (127 ± 2.5 Ω/□) and CNT sheet (96 ± 1.92 Ω/□), respectively. The average sheet resistivity measured for ten CNT-PI films (0.5 × 4 cm^2) was 187 ± 41 Ω/□. The film sheet resistivity can be converted to volume resistivity of 0.2 ± 0.04 Ωcm (for the 9 ± 2 μm thick conductive layer), an enhancement of 18 orders of magnitude compared to pristine PI, with sheet resistivity of 1.5 × 10^{17} Ωcm.[31]

The sheet resistivity of the CNT-PI films was found to be about 50% higher than that of the pristine CNT sheets. The fact that the sheet conductivity was preserved in spite of the insulative PI infiltration implies that the electrical current was enabled through the original entangled CNT network that was not interrupted by the insulative PI. This proves that the polymer solution did not penetrate into the interface at the CNT junctions and so the original continum of ohmic contacts between adjacent CNTs was preserved. This is in contrast to CNT-PI composites that are produced by CNT dispersion in a polymer matrix.[4]

Measuring the resistance for an increasing number of segments serves not only for extraction of the contact resistance but also for investigation of the homogeneous morphology along the samples. According to relation 1, the resistance of a homogeneous film should be characterized by a linear increase of the sheet resistance with the number of segments, L/w. Indeed, the sheet resistance of both the pristine CNT sheet and CNT-PI film showed linear behavior (Figure 3b). This result suggests that the CNT sheets were homogeneous after the CVD procedure and its uniform nature was preserved after PI infiltration.

The mechanism that governs the sheet resistivity was investigated by additional electrical characterizations along the lateral direction, current versus voltage, and temperature-dependent measurements. Current versus voltage curves were obtained at room temperature along the lateral direction of the bottom surface of CNT-PI films. The voltage was measured for varying DC current in the range between −30 and 30 mA (Figure 3c). The current versus voltage curves showed an ohmic behavior at room temperature, similar to that found in the vertical direction (Figure 3a), indicating direct contact between the CNTs.

The temperature dependence of the sheet resistivity was measured by four-point van der Pauw method. The sheet resistivity was measured for 5 × 5 mm^2 samples at −160 to 200 °C. Both CNT-PI films and pristine CNT sheets were tested, as depicted in Figure 3d with red squares and black triangles, respectively. The data exhibited conduction behavior that corresponds to the variable range hopping (VRH) conduction mechanism. The VRH mechanism is described by

$$\rho_s T^{-1/2} \propto \exp(B/T^{1/4}) \quad (2)$$

where ρ_s is the sheet resistivity, T is the temperature, and B is a constant. The data was plotted as Arrhenius curves of $\ln(\rho_s T^{-1/2})$ versus $T^{-1/4}$ with fitted linear trend lines. This behavior is related to the lack of covalent bonding between the stacked cones that characterizes the CSCNT structure. Therefore, electrons hop from one defect site to another and between neighboring CNTs. The samples were finally cooled to 25 °C and their resistivities increased back to their original values with no indication of hysteresis (data not shown).

The difference between the room temperature resistivity of both samples is expressed by the offset of the pristine CNT sheet and CNT-PI film plots. This was expected since the room temperature resistivity of the CNT-PI film is higher than that of the pristine CNT sheet, as shown in Figure 3b. A similarity of the temperature-dependent resistivity of both samples is evident by the similar slope of both trend lines. This result implies that the resistivity change is an inherent characteristic of the CNTs and cannot be related to the PI.

The fact that the PI matrix did not influence the resistivity temperature dependence can be attributed to the excellent thermal stability of the PI. Polymer matrices with inferior thermal stability tend to reduce their modulus and turn into rubber-like material at temperatures close to their glass transition region, thus affecting the composite electrical conductivity.[32] As mentioned above, this effect was not observed in the case of a PI matrix because of its high thermal stability that is expressed in its high glass transition region of 360−410 °C.[31] Furthermore, during heating to 200 °C, PI is expected to expand according to a thermal expansion coefficient of 32 μm/m-K (related to temperature range of 100−200 °C).[31] Yet, no effect of the PI matrix on the temperature-dependent resistivity was observed. We assume that the ohmic nature of the intertube contact was preserved

since the matrix expansion was reflected by CNT bending rather than intertube separation.

Next, the durability of the electrical conductivity of the CNT-PI film under mechanical manipulations was examined. The sheet resistivity of the CNT-PI film was noted by ρ_{s0} for the original film, and ρ_s for the manipulated film. The total sheet resistivity change in percentage, $\Delta\rho_s$, was calculated by

$$\Delta\rho_s = \left(\frac{\rho_s - \rho_{s0}}{\rho_{s0}}\right)\cdot 100\% \quad (3)$$

CNT-PI films (0.5 × 4 cm^2) were wound 300 times around a ceramic rod of 2.9 mm diameter (Figure 4, inset). The sheet resistivity was measured after each set of windings. This flexibility test is considered severe due to the small bending diameter in comparison to previous publications.[33] Figure 4 shows the total sheet resistivity change in percentage versus times of windings. The error bars reflect 10 repetitions for each resistivity measurement. The resistivity was found to be stable with insignificant increase of about 3% after 300 winding cycles, among the smallest resistivity changes under bending reported to date.[33] This is in contrast to fragile commercial conducting coatings, such as ITO, that typically suffer from severe degradation of the electrical conductance due to fracture of the coating upon bending.[3] Previously studied space-durable CNT-coated PI films[34] were tested for conductivity robustness after 4 folding cycles and showed insignificant changes in conductivity. The conductivity of these films was preserved as well after crumpling the samples into a ball.

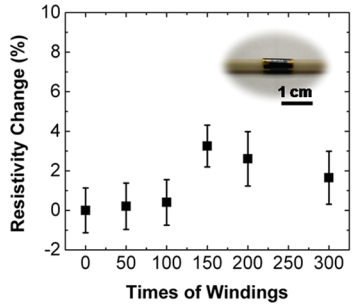

Figure 4. Total sheet electrical resistivity change as a function of the number of winding cycles for a CNT-PI film. Inset: A free-standing CNT-PI film (17 μm thick, 0.5 × 4 cm^2 area) wound around a 2.9 mm diameter rod.

3.3. Durability in Space Environment. The developed CNT-PI nanocomposites may be considered as an alternative for the ESD protection layer of spacecraft thermal control blankets for GEO orbits. As an outer layer, the CNT-PI film is directly exposed to the charged environment during the length of the mission (10−15 years) and hence the preservation of its electrical conductivity is crucial to attain ESD protection. The compatibility of the CNT-PI films for space applications was examined under simulated space environment, including effects of vacuum, thermal cycles, and ionizing radiation.

Materials under vacuum environment release a volatile content that might contaminate adjacent surfaces. The behavior of CNT-PI films under vacuum was measured according to ASTM E595-07,[24] resulting in TML of 0.588% and CVCM of 0.004%. As these values are lower than that of the low-outgassing criterion, the CNT-PI films are not considered a contamination threat and hence they are approved for vacuum environment.

The equilibrium temperature, T (K), of a CNT-PI film in space is governed by the heat it absorbs from the sun and the heat it emits to its surroundings. It was calculated by[1]

$$T = \left(\frac{\alpha_s}{\varepsilon}\right)^{1/4}\left(\frac{SA_n}{\sigma A}\right)^{1/4} \quad (4)$$

where α_s is related to the film's solar absorptance, ε is its emittance, S (W/m^2) is the solar flux per unit area at the spacecraft orbit, A_n (m^2) is the film's surface area normal to the solar flux, A (m^2) is its total surface area, and σ (5.67 × 10^{-8} W/m^2 K^4) is the Stefan−Boltzmann constant. The maximal temperature calculation was related to a solar flux, S, of 1366.1 W/m^2, the average value above earth atmosphere at 1 AU distance.[35] The thermo-optical properties of the CNT-PI films are also required for the maximal temperature calculation and hence they were measured, resulting in solar absorptance, α_s, and emittance, ε, values of 0.99 and 0.86, respectively. A maximal temperature of 135 °C was evaluated by substituting S, α_s, and ε. CNT-PI film function under extreme thermal cycles was investigated according to the computed maximal temperature. CNT-PI films (5 × 5 mm^2) were subjected to 29 thermal cycles of −100 to 140 °C using a temperature controlled stage in nitrogen atmosphere. The sheet resistivity of the films was measured by four-point van der Pauw method at the minimal and maximal temperatures for every second cycle (Figure 5a). Stability of the electrical conductivity under thermal cycles was demonstrated, indicating compatibility for CNT-PI film performance under space environment.

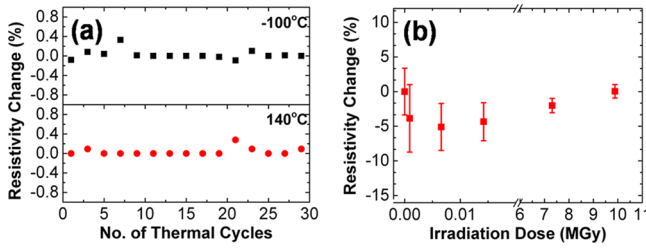

Figure 5. Sheet resistivity change of CNT-PI film (a) as a function of number of thermal cycles at −100 and 140 °C and (b) as a function of γ radiation dose.

The incorporation of CNTs into the PI matrix resulted in an increase in the thermo-optical properties α_s and ε. Specifically, α_s increased by 100% due to the 14 vol % CNT content. This phenomenon is well-known for previously studied CNT-PI films[12] for space applications, where an absorptance increase by a factor of 5 was reported at CNT loading of 0.08 wt %.

Thermal blankets are composed of multiple reflective layers that contribute to the close to 100% radiation insulation.[36] For proper thermal management in the satellite, the total layered structure of the thermal blanket is required to demonstrate low α_s and high ε. The CNT-PI film is suggested herein as the outer layer for ESD protection of the thermal blanket. The impact of the high α_s of the CNT-PI outer layer on the total performance of the layered blanket is negligible.

Another space environment hazard is ionizing radiation in GEO, an orbit that is generally simulated by gamma irradiation. To explore the film durability, CNT-PI films (0.5 × 4 cm^2) were exposed to γ radiation using a ^{60}Co source. The sheet

resistivity was measured as a function of gamma irradiation dose as shown in Figure 5b. Minor decrease in the CNT-PI film resistivity was observed under low irradiation doses. The resistivity increased back to its original value under high irradiation doses. The sheet resistivity of the films exhibited insignificant changes under 9.9 MGy, an equivalent irradiation dose to mission duration (15 years). The error bars were plotted according to 7 measurements. Although the space durability of CNTs and CNT-based composites was tested previously,[25,26,37] the electrical conductivity durability under ionizing irradiation is demonstrated here for the first time.

4. SUMMARY AND CONCLUSIONS

Electrically conducting and flexible CNT-PI films for space applications were developed using polymer solution infiltration into CVD-grown entangled CNT sheets with cup-stacked nanostructure. The fabrication process prevents CNT agglomeration and degradation of the CNT properties that are common in dispersion-based processes. CNT-PI films were produced demonstrating high lateral and top-to-bottom ohmic conductivities at room temperature. CNT-PI films with sheet resistivity of as low as 122 Ω/□ were obtained, preserving the original CNT sheet resistivity. An electrical conductance mechanism was suggested, demonstrating that the PI did not penetrate into the interface at the CNT junctions, resulting in minimal interface resistance and high sheet conductivity, thus maintaining the original conductance of the CNT network. Additionally, the electrical conductivity was found to be stable under thermal and mechanical manipulations. Moreover, the CNT-PI films were tested under simulated space environment and found to be durable for GEO space applications, considering hazards such as vacuum, thermal cycles, and ionizing radiation. Further research is needed to establish the suitability of CNT-PI films for low earth orbit (LEO) environment, where atomic oxygen is dominant. Additionally, CNT-PI films with higher electrical conductivity can be achieved by increasing the density of the original entangled CNT sheets. Reducing the pore volume and improving the packing density can be controlled by the CVD procedure, while enhanced electrical conductivity of cup-stacked CNTs can be achieved after annealing[38] for further optimization. Overall, CNT-PI infiltrated composites offer an interesting route toward utilization of CNTs in space applications, in particular for ESD protection.

■ AUTHOR INFORMATION

Corresponding Author

*Tel: +972-8-943-4437. E-mail: nurita@soreq gov.il.

Notes

The authors declare no competing financial interest.

■ ACKNOWLEDGMENTS

The authors thank Moshe David-Pur for the CVD growth of the CNT sheets and Dr. Judith Grinblat for the TEM analysis. The authors acknowledge Sapir Glam, Aviya Edri, Amnon Zentner, and Meital Ozeri for experimental assistance. The authors thank Isaac Balberg, Oded Milo, and Doron Azulai for useful discussions.

■ REFERENCES

(1) Tribble, A. C. *The Space Environment*; Princeton University Press: Princeton, NJ, 1995.

(2) Ghosh, M.; Mittal, K. *Polyimides: Fundamentals and Applications*; Marcel Dekker: New York, NY, 1996.

(3) Cairns, D. R.; Witte, R. P.; Sparacin, D. K.; Sachsman, S. M.; Paine, D. C.; Crawford, G. P.; Newton, R. Strain-Dependent Electrical Resistance of Tin-Doped Indium Oxide on Polymer Substrates. *Appl. Phys. Lett.* **2000**, *76*, 1425−1427.

(4) Ma, P. C.; Siddiqui, N. A.; Marom, G.; Kim, J. K. Dispersion and Functionalization of Carbon Nanotubes for Polymer-Based Nanocomposites: A Review. *Composites, Part A* **2010**, *41*, 1345−1367.

(5) Terrones, H.; Hayashi, T.; Muñoz-Navia, M.; Terrones, M.; Kim, Y. A.; Grobert, N.; Kamalakaran, R.; Dorantes-Dávila, J.; Escudero, R.; Dresselhaus, M. S.; Endo, M. Graphitic Cones in Palladium Catalysed Carbon Nanofibres. *Chem. Phys. Lett.* **2001**, *343*, 241−250.

(6) Kim, T.-H.; Wendelken, J. F.; Li, A.-P.; Du, G.; Li, W. Probing Electrical Transport in Individual Carbon Nanotubes and Junctions. *Nanotechnology* **2008**, *19*, 485201.

(7) Liu, Q.; Ren, W.; Chen, Z.-G.; Yin, L.; Li, F.; Cong, H.; Cheng, H.-M. Semiconducting Properties of Cup-Stacked Carbon Nanotubes. *Carbon* **2009**, *47*, 731−736.

(8) Glatkowski, P. J. In *Carbon Nanotube Based Transparent Conductive Coatings*; Citeseer, The Pennsylvania State University: University Park, PA, 2003; pp 2146−2152.

(9) Jiang, X.; Bin, Y.; Matsuo, M. Electrical and Mechanical Properties of Polyimide−Carbon Nanotubes Composites Fabricated by in Situ Polymerization. *Polymer* **2005**, *46*, 7418−7424.

(10) Ogasawara, T.; Ishida, Y.; Ishikawa, T.; Yokota, R. Characterization of Multi-Walled Carbon Nanotube/Phenylethynyl Terminated Polyimide Composites. *Composites, Part A* **2004**, *35*, 67−74.

(11) Ounaies, Z.; Park, C.; Wise, K.; Siochi, E.; Harrison, J. Electrical Properties of Single Wall Carbon Nanotube Reinforced Polyimide Composites. *Compos. Sci. Technol.* **2003**, *63*, 1637−1646.

(12) Smith, J.; Connell, J.; Delozier, D.; Lillehei, P.; Watson, K.; Lin, Y.; Zhou, B.; Sun, Y. P. Space Durable Polymer/Carbon Nanotube Films for Electrostatic Charge Mitigation. *Polymer* **2004**, *45*, 825−836.

(13) Zhu, B. K.; Xie, S. H.; Xu, Z. K.; Xu, Y. Y. Preparation and Properties of the Polyimide/Multi-Walled Carbon Nanotubes (Mwnts) Nanocomposites. *Compos. Sci. Technol.* **2006**, *66*, 548−554.

(14) Yuan, W.; Che, J.; Chan-Park, M. B. A Novel Polyimide Dispersing Matrix for Highly Electrically Conductive Solution-Cast Carbon Nanotube-Based Composite. *Chem. Mater.* **2011**, *23*, 4149−4157.

(15) Cebeci, H.; Villoria, R. G.; Hart, A. J.; Wardle, B. L. Multifunctional Properties of High Volume Fraction Aligned Carbon Nanotube Polymer Composites with Controlled Morphology. *Compos. Sci. Technol.* **2009**, *69*, 2649−2656.

(16) Jung, Y. J.; Kar, S.; Talapatra, S.; Soldano, C.; Viswanathan, G.; Li, X.; Yao, Z.; Ou, F. S.; Avadhanula, A.; Vajtai, R. Aligned Carbon Nanotube-Polymer Hybrid Architectures for Diverse Flexible Electronic Applications. *Nano Lett.* **2006**, *6*, 413−418.

(17) Peng, H.; Sun, X. Highly Aligned Carbon Nanotube/Polymer Composites with Much Improved Electrical Conductivities. *Chem. Phys. Lett.* **2009**, *471*, 103−105.

(18) Jiang, Q.; Wang, X.; Zhu, Y.; Hui, D.; Qiu, Y. Mechanical, Electrical, and Thermal Properties of Aligned Carbon Nanotube/Polyimide Composites. *Composites, Part B* **2014**, *56*, 408−412.

(19) David-Pur, M.; Bareket-Keren, L.; Beit-Yaakov, G.; Raz-Prag, D.; Hanein, Y. All-Carbon-Nanotube Flexible Multi-Electrode Array for Neuronal Recording and Stimulation. *Biomed. Microdevices* **2013**, *16*, 43−53.

(20) Tb, Pyralin Polyimide Coating Pi 2545 Pi 2540, Product Information, Du-Pont. Inc, February 1993.

(21) Verker, R.; Grossman, E.; Eliaz, N. Erosion of Poss-Polyimide Films under Hypervelocity Impact and Atomic Oxygen: The Role of Mechanical Properties at Elevated Temperatures. *Acta Mater.* **2009**, *57*, 1112−1119.

(22) Horcas, I.; Fernandez, R.; Gomez-Rodriguez, J.; Colchero, J.; Gómez-Herrero, J.; Baro, A. Wsxm: A Software for Scanning Probe Microscopy and a Tool for Nanotechnology. *Rev. Sci. Instrum.* **2007**, *78*, 013705−013705−8.

(23) van der Pauw, L. A Method of Measuring Specific Resistivity and Hall Effect of Discs of Arbitrary Shape. *Philips Res. Rep.* **1958**, *12*, 1−9.
(24) *Standard Test Method for Total Mass Loss and Collected Volatile Condensable Materials from Outgassing in a Vacuum Environment*, ASTM E595-07; ASTM International: West Conshohocken, PA, 2007.
(25) Lubkowski, G.; Kuhnhenn, J.; Suhrke, M.; Weinand, U.; Endler, I.; Meibner, F.; Richter, S. Gamma Radiation Effects in Vertically Aligned Carbon Nanotubes. *IEEE Trans. Nucl. Sci.* **2012**, *59*, 792−796.
(26) Nielsen, K. L.; Hill, D. J.; Watson, K. A.; Connell, J. W.; Ikeda, S.; Kudo, H.; Whittaker, A. K. The Radiation Degradation of a Nanotube−Polyimide Nanocomposite. *Polym. Degrad. Stab.* **2008**, *93*, 169−175.
(27) Holmes-Siedle, A.; Adams, L. *Handbook of Radiation Effects*; Oxford University Press: Oxford, U.K., 1993.
(28) Kiselev, N.; Musatov, A.; Kukovitskii, E.; Hutchison, J.; Zhigalina, O.; Artemov, V.; Grigoriev, Y. V.; Izrael'yants, K.; L'vov, S. Influence of Electric Field and Emission Current on the Configuration of Nanotubes in Carbon Nanotube Layers. *Carbon* **2005**, *43*, 3112−3123.
(29) Nolan, P. E.; Lynch, D. C.; Cutler, A. H. Carbon Deposition and Hydrocarbon Formation on Group VIII Metal Catalysts. *J. Phys. Chem. B* **1998**, *102*, 4165−4175.
(30) Al-Saleh, M. H.; Sundararaj, U. A Review of Vapor Grown Carbon Nanofiber/Polymer Conductive Composites. *Carbon* **2009**, *47*, 2−22.
(31) Du Pont, Kapton Hn Polyimide Film, K-15345−1 Technical Data Sheet, Apr. 2011.
(32) Mohiuddin, M.; Hoa, S. Temperature Dependent Electrical Conductivity of Cnt−Peek Composites. *Compos. Sci. Technol.* **2011**, *72*, 21−27.
(33) Zhu, Y.; Sun, Z.; Yan, Z.; Jin, Z.; Tour, J. M. Rational Design of Hybrid Graphene Films for High-Performance Transparent Electrodes. *ACS Nano* **2011**, *5*, 6472−6479.
(34) Watson, K. A.; Ghose, S.; Delozier, D. M.; Smith, J. G.; Connell, J. W. Transparent, Flexible, Conductive Carbon Nanotube Coatings for Electrostatic Charge Mitigation. *Polymer* **2005**, *46*, 2076−2085.
(35) *Standard Solar Constant and Zero Air Mass Solar Spectral Irradiance Tables*, ASTM E490; ASTM International: West Conshohocken, PA, 2002.
(36) Finckenor, M.; Dooling, D., Multilayer Insulation Material Guidelines, April 1999.
(37) Li, B.; Feng, Y.; Ding, K.; Qian, G.; Zhang, X.; Zhang, J. The Effect of Gamma Ray Irradiation on the Structure of Graphite and Multi-Walled Carbon Nanotubes. *Carbon* **2013**, *60*, 186−192.
(38) Endo, M.; Lee, B.; Kim, Y.; Kim, Y.; Muramatsu, H.; Yanagisawa, T.; Hayashi, T.; Terrones, M.; Dresselhaus, M. Transitional Behaviour in the Transformation from Active End Planes to Stable Loops Caused by Annealing. *New J. Phys.* **2003**, *5*, 121.